Indonesian Journal of Maritime Technology (ISMATECH)
Vol. 04, Issue 01, June 2026
eISSN: 3025-518X
DOI: https://doi.org/10.35718/ismatech.v4i1.8481960

Computational Fluid Dynamics Analysis of Breakwater Configurations for Enhanced Coastal Resilience in North Java

Alif Nur Rochmad[1*], Muhamad Rakif Panguale[1], Muhamad Saiful Rahman Hamka[1], Septaviola Dini Utami[1]

[1]Department of Shipbuilding Engineering, Shipbuilding Institute of Polytechnic Surabaya, Surabaya, 60111, Indonesia

KEYWORDS
Breakwater;
CFD;
Coastal Protection;
Wave Attenuation;
North Java

ABSTRACT – The North Java shoreline, much like coastlines elsewhere in the world, continues to suffer the cumulative effects of coastal erosion and storm surge, and breakwaters remain the principal line of defense against this incoming wave energy. A substantial number of these structures, however, are still sized and shaped using generic rules of thumb instead of being calibrated to site-specific wave conditions and seabed characteristics, and the body of published work that tests breakwater configurations against actual North Java conditions is still limited. The present study closes part of that gap by applying a Computational Fluid Dynamics (CFD) simulation framework to examine how breakwater geometry, porosity, and layout govern hydrodynamic behavior under representative wave loading. The free surface and the wave-structure interaction were resolved using the Volume of Fluid (VOF) approach, paired with a turbulence closure model appropriate for free-surface flow. Over the course of the simulated runs, the configurations under investigation brought wave height down from 1.25 m to roughly 0.45 m by t = 20 s. The seaward face experienced its largest dynamic pressure, 38.7 kPa, at t = 10 s, a moment that also coincided with the highest overtopping velocity of 3.42 m/s, even as flow inside the sheltered zone fell to only 0.22 m/s, a rate low enough to let sediment settle out. A subsequent sensitivity analysis showed that raising porosity by 10% together with a gentler slope gradient lowered the peak structural pressure by as much as 15%, yielding design guidance with practical relevance for North Java and comparable coastal settings.

*Corresponding Author | Alif Nur Rochmad | ✉ (alifrochmad798@gmail.com)

INTRODUCTION

Coastlines worldwide face mounting pressure from natural forces. Relentless wave action, storm surges, and a steadily rising sea level have together sped up erosion, degraded infrastructure, and left coastal communities and ecosystems more vulnerable than before. Among the various tools engineers rely on to counter these forces, the breakwater remains a recurring choice [1]. Positioned offshore or close to the shoreline, it intercepts and dissipates wave energy, lowers wave height, and produces a calmer zone in its lee that benefits vessels, port activities, or simply guards the coastline against erosion. Even so, designing such a structure is far from straightforward. Doing it well demands a solid grasp of wave-structure interaction, the loads involved, and the patterns by which sediment moves and resettles around the structure [2].

Breakwater design has long rested on three traditional pillars: empirical formulas, scaled physical models, and sustained field observation. Each pillar offers genuine benefits, yet each carries a price as well. Physical testing is costly, scaled models introduce their own scale-effect distortions, and neither approach fully reproduces how unpredictable actual flow conditions can become. Over recent decades, Computational Fluid Dynamics (CFD) has transformed this field, maturing into a numerical tool that reproduces detailed flow and wave behavior at relatively low cost. Through it, engineers can trace a wave as it propagates, breaks, runs up, and reflects, while capturing the forces acting on a structure at high resolution in both space and time [3]. Given this, it comes as no surprise that CFD has become a preferred method for examining breakwater performance and stability across varied wave conditions, supporting the design decisions on which coastal protection ultimately depends [26].

CFD has been applied by researchers to nearly every dimension of breakwater behavior, ranging from the structure's basic geometry to its response under varying water conditions. Particular shapes have attracted close attention. A semi-circular breakwater layout, for example, was simulated with CFD to evaluate how effectively it suppresses incoming waves [4], and a CFD-based design procedure has likewise been put forward for rubble-mound breakwaters, structures that retain their popularity thanks to construction flexibility and robust energy-dissipation performance [5]. Work of this kind shows how easily CFD enables different geometries to be set against one another on a single practical measure: how well each one removes wave energy.

The reach of CFD goes well beyond breakwaters built purely to block waves. Take, for instance, the full-scale U-OWC (Oscillating Water Column) breakwater, which researchers have modeled to examine both its hydrodynamic behavior and its capacity to harvest wave energy while continuing to shield the coast [6]. Another strand of research looks at the interface between a breakwater and its foundation, using a coupled FEMDEM-CFD scheme so that large armor units respond to wave loading more realistically [7]. Caisson breakwaters under severe wave loading have been studied in a comparable way, with a combined CFD/DEM approach applied to capture how fluid, structure, and soil interact [8].

Floating breakwaters form another distinct family of structures, typically chosen for deeper water or softer seabed conditions, and CFD has likewise made significant contributions in this area. In one notable example, CFD was combined with a multi-objective genetic algorithm to optimize a floating breakwater, demonstrating how computation can steer a design toward a leaner, more adaptable outcome [9]. Cylindrical floating breakwaters, for their part, have been investigated through CFD to gauge how effectively they restrain sediment transport, a far from trivial concern in coastal engineering [10].

Pairing breakwaters with wave energy converters (WECs) reflects a wider trend toward coastal infrastructure designed to serve more than a single function. CFD has been used to study a pivoted point-absorber WEC built into a breakwater, balancing its energy-conversion potential against its hydrodynamic behavior [11], as well as a heaving WEC coupled with a breakwater, where the payoff comes in the form of calmer water alongside electricity generation [12]. Even the breakwater's most basic role of dissipating wave energy has been investigated through CFD across several configurations to clarify precisely how that energy reduction takes place [13].

Viewed collectively, this literature shows the extent to which CFD has come to pervade breakwater research, covering fixed, floating, and multi-functional designs alike, and tackling issues that range from basic wave attenuation through to the more intricate structural and environmental effects that lie beneath it.

Notwithstanding this considerable volume of work, surprisingly few studies have set breakwater configurations directly against one another under the specific conditions of a regional coastline such as North Java. Generic breakwater types are thoroughly documented, but detailed work that adjusts porosity, crest width, submerged depth, or multi-unit layouts to match a particular region's wave climate, bathymetry, and sediment characteristics is still uncommon [14]. A further limitation is that much existing research concentrates on a single breakwater type or a narrow band of parameters, so the question of how a full set of design parameters interacts to shape overall performance at one specific location, while weighing wave attenuation against side effects such as sediment movement, remains largely unaddressed. This leaves a substantial gap in the capacity to design breakwaters that are not just well engineered in a generic sense, but genuinely matched to the locations where they will stand.

Owing to its distinctive wave climate, shallow water, and substantial exposure to erosion, the North Java coast demands coastal protection that is both effective and long-lasting [27]. Designs drawn from generic principles, or simply carried over from other regions, may not transfer well to this setting; they risk falling short in performance, raising maintenance costs, or producing unintended environmental consequences. What is plainly required is an understanding of how various breakwater configurations actually perform under North Java's particular conditions, so that future designs can become more efficient, more resilient, and more environmentally sound. Until such configurations are rigorously tested with tools like CFD, much of the potential for improved, locally calibrated designs remains untapped [15].

CFD modeling of breakwaters depends on numerical methods able to handle multiphase air-water flow. The Volume of Fluid (VOF) method is typically chosen for tracking the free surface and wave breaking, while turbulence closures such as k-ϵ or k-ω SST account for the energy dissipated in the vicinity of the structure. Coupling CFD with the Discrete Element Method (DEM) or the Finite Element Method (FEM) goes a step further, capturing the combined fluid-structure-soil response that is so significant in rubble-mound and caisson breakwaters [16]. High-performance computing (HPC) makes it practical to simulate full-scale structures and longer wave trains, which lends greater realism to the resulting outputs. Post-processing subsequently enables wave transmission, reflection, energy dissipation, and structural forces to be inspected in fine detail. Layering optimization techniques such as multi-objective genetic algorithms on top of these simulations further widens the search for favorable configurations across a large parameter space.

The model adopted for this research was built using CFD software. A two-dimensional domain representing a cross-section of the North Java coast was constructed, with boundary conditions configured for both wave generation and wave absorption, while the free surface and wave-structure interaction were handled through the Volume of Fluid (VOF) method. Each breakwater configuration was specified by varying crest width, freeboard, submerged depth, and porosity, while the incident wave height, period, and water depth were chosen to reflect both typical and extreme conditions along the North Java coast. Transmission and reflection coefficients, along with energy-dissipation rates, were then derived for every configuration, after which pressure distributions and structural forces were examined to evaluate stability, ultimately producing design-relevant insights for breakwaters intended for the North Java coast [17].

METHODS

This study draws on Computational Fluid Dynamics (CFD) to examine the hydrodynamic performance of several breakwater configurations. CFD makes it possible to study the wave-structure interaction underlying coastal protection against erosion and storm surge in a detailed and controlled fashion [18]. The following sections lay out the research object and how it was treated, the numerical methods and procedures applied, and the tools and materials involved [19].

Research Object

The object at the center of this research is the breakwater itself, with particular attention given to two distinct geometric designs, the existing breakwater designs, illustrated in Figure 1. These two designs embody different structural layouts intended to protect the coastline. The source file records a Number of Stones, which relates to the structure's actual construction, but within the simulation the breakwater is represented as a defined geometric shape interacting with the surrounding flow [20].

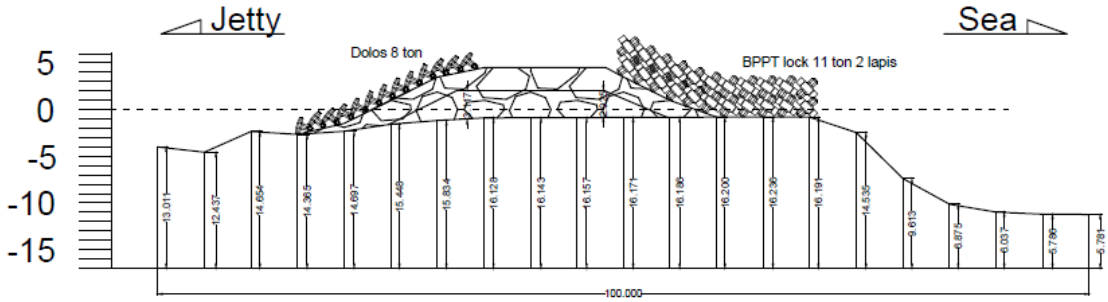

Figure 1. Breakwater

Positioned offshore or close to the shoreline, a breakwater protects a coastline or harbour basin by intercepting incoming waves and absorbing or reflecting a portion of their energy, leaving calmer water and visibly smaller waves in its wake. Within this CFD study, the structure is treated as a solid, impermeable body with a fixed shape [21].

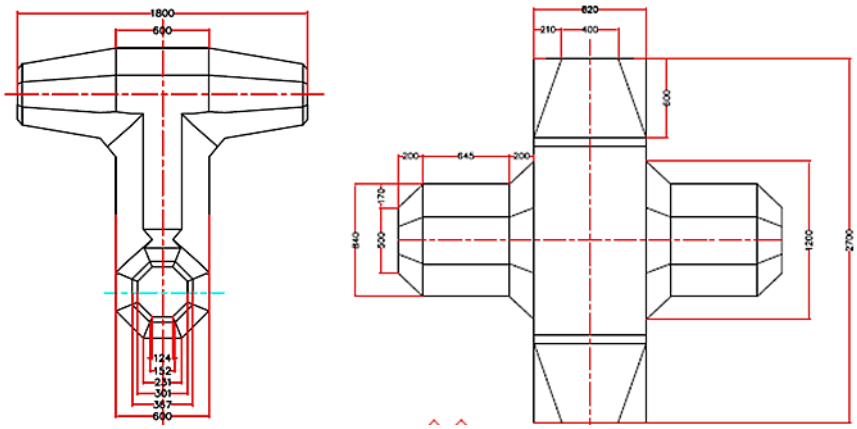

Figure 2. Breakwater stones (Dolos and BPPT Lock)

Figure 2 shows the cross-sectional drawing that acts as the foundational blueprint for the breakwater's stone geometry. It is worth noting, however, that specific details regarding the constituent rock types, such as density, porosity, or precise size distribution, were unavailable. The breakwater is therefore modeled as a "wall" within the boundary conditions, standing in for a rigid, non-deformable barrier to fluid flow.

Every piece of research data in this study was generated solely through computational means. Instead of drawing on field measurements or physical model testing, the results came directly from the CFD simulation runs: the computational domain is set up, the breakwater geometry is defined, a range of wave conditions is applied, and quantitative output is then extracted. That output covers pressure distributions, velocity fields, wave heights, and other relevant quantities drawn from the flow field. Because the entire process is computed numerically, a broad range of scenarios and configurations can be tested in a controlled setting, sparing the substantial cost and effort that physical model testing usually demands [22].

Treatment of the Research Object

The research object was handled by establishing which parameters would be held fixed and which would be varied, allowing the breakwater's hydrodynamic performance to be studied in a controlled and repeatable manner.

Certain parameters were held constant across the runs so that the effect of the varying ones could be isolated. The breakwater geometry (Design) stayed fixed within each set of runs, with its dimensions, crest width, height, and slope taken directly from the drawings. Domain size was likewise kept unchanged so that wave propagation and interaction remained consistent [23].

Figure 3. Geometry Configuration

As shown in Figure 3, the inlet is positioned three breakwater lengths (3L) upstream of the structure, equivalent to 80 meters, while the outlet sits one length (1L) downstream. The top boundary is set 0.5L above the breakwater to allow room for the wave crests. This domain size ensures the incident waves are fully developed before reaching the breakwater while preventing outlet reflections from disturbing the region of interest. The same approach carries through to the mesh, with a global element size of 1 meter serving as the baseline resolution.

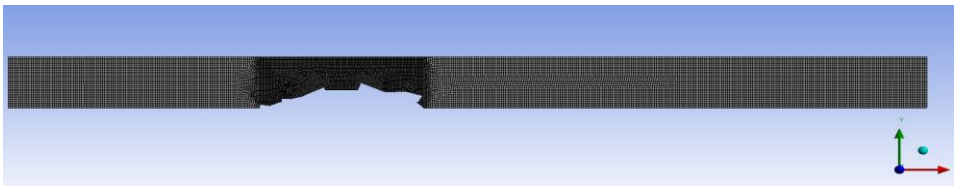

Figure 4. Mesh Configuration

In the area surrounding the breakwater, where accuracy is most critical, a finer local mesh size of 0.5 meters was applied. This refinement, depicted in Figure 4, yields 17,713 elements and 18,257 nodes, which keeps the computational cost manageable while still resolving the flow near the structure adequately. Air-water interaction is handled through the Volume of Fluid (VOF) model, with the "Open Channel Flow" and "Open Channel Wave BC" options switched on (Figure 5). The VOF formulation used is "Explicit" combined with "Sharp" interface modeling to maintain a clearly defined air-water interface. The reference wave direction is fixed at a mean heading angle of 0 degrees, meaning waves approach the breakwater perpendicularly.

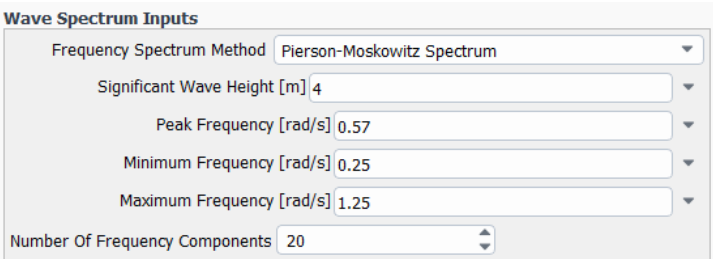

Figure 5. Wave configuration

At the core of the study lies the set of variable parameters, which allow the breakwater's response to be examined across different conditions. The incident wave is specified through a single significant wave height of 4 meters, adopted as the design wave for this area. The waves produced in the simulation are "random waves," represented through the Pierson-Moskowitz Spectrum (Figure 5).

A key variable here is the bottom level specified within the wave boundary condition, which determines the water depth. For the 4 m significant wave height, the bottom level is set at 0 meters; combined with a free surface level of 8.09 meters, this yields a water depth of 8.09 meters, falling within the intermediate-water range characteristic of the North Java coast.

Establishing the domain represents an essential initial step. As mentioned earlier, its size is fixed in proportion to the breakwater length (L): the inlet at 3L upstream, the outlet at 1L downstream, and the top boundary at 0.5L above the structure. The bottom boundary, in turn, is determined by the "Bottom Level" specified in the wave

boundary conditions. These choices ensure incident waves remain fully developed and steady before reaching the breakwater, while also preventing outlet reflections from disturbing the area surrounding the structure [24].

Numerical Method and Procedures

Computational Fluid Dynamics (CFD) serves as the primary method underpinning this research. The governing equations of fluid motion are discretized across a computational mesh, then solved numerically to reproduce the behavior of water and air under the specified conditions. The solver carries out the iterative calculations required to track how the incoming wave field evolves as it meets the breakwater surfaces defined by the boundary conditions.

In recent years, CFD has emerged as a practical alternative to physical flume testing within coastal and ocean engineering, particularly for examining wave-structure interaction. For the problem considered here, it offers several distinct advantages. First, it allows velocity, pressure, turbulence, and free-surface fields around the structure to be resolved at a level of detail considerably finer than what physical-model instruments typically achieve. Second, once the model has been established, modifying the geometry or the incident wave conditions becomes relatively inexpensive, an advantage well matched to the configuration-based study carried out here. The simulation also runs at full scale, thereby sidestepping the scale effects that frequently complicate small physical models. Finally, post-processing makes it possible to view the computed flow fields directly, which proves valuable in interpreting how the breakwater dissipates incoming wave energy.

Even so, these advantages are accompanied by limitations that deserve acknowledgment. A multiphase, free-surface domain at this scale places substantial demand on memory and computational run time. The resulting output is also sensitive to the modeling choices made, particularly with respect to turbulence and multiphase settings, as well as to mesh quality, since an excessively coarse grid risks distorting the predicted forces. A grid was therefore selected carefully, weighing computational cost against the resolution needed. Furthermore, the reliability of any CFD output ultimately depends on validation; the values reported here should accordingly be regarded as numerical estimates that would benefit from further comparison against measured or analytical data.

Because the flow involves two immiscible fluids, air and water, a multiphase formulation is required, which is exactly why the Volume of Fluid (VOF) model was selected (Figure 5). VOF suits this problem well because its core principle is tracking the location of the air-water interface and how that interface moves as waves run up and break against the structure. The "Number of Eulerian Phases" was accordingly set to 2, representing air and water. The "Formulation" chosen was "Explicit," generally the more stable option for transient free-surface flows of this type. For "Interface Modeling," the "Sharp" setting was used to preserve a clearly defined air-water boundary, an essential condition for capturing both wave propagation and breaking behavior. Meanwhile, the "Open Channel Flow" and "Open Channel Wave BC" settings were employed to reproduce the gravity-driven free-surface flow together with the incoming wave train.

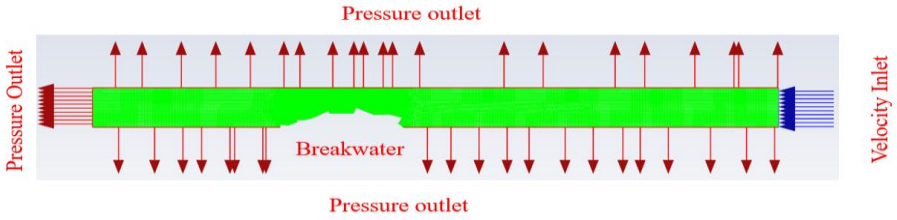

Figure 6. Boundary Condition

Boundary conditions specify how the fluid behaves at each edge of the domain (Figure 6). The inlet takes the form of a "Velocity Inlet" combined with "Open Channel Wave BC," where the incident waves are generated and introduced into the domain; the corresponding wave settings appear below. The outlet is configured as a "Pressure Outlet," allowing fluid to exit at a fixed static pressure, generally atmospheric, while helping to damp reflections that would otherwise compromise the results. The breakwater itself is defined as a "Wall" with a no-slip condition, meaning the velocity at its surface is zero and it remains impermeable to the flow; the side facing the waves is labeled the "seaside" and the opposite side the "portside." The top boundary is likewise a "Pressure Outlet," permitting air to move in and out so that pressure remains atmospheric as the free surface rises and falls.

Incident waves are introduced at the "Velocity Inlet" through the "Open Channel Wave BC" settings (Figure 5). The spectrum follows the Pierson-Moskowitz form, a widely used description of a fully developed sea across a broad band of frequencies. Expressed in terms of angular frequency, significant wave height, and peak angular frequency, it takes the form [25]:

$$S(\omega) = \frac{5}{16} H_s^2 \omega_p^4 \omega^{-5} \exp\left(-\frac{5}{4}\left(\frac{\omega_p}{\omega}\right)^4 \right) \quad (1)$$

where ω_p is related to the peak period T_p by $\omega_p = \frac{2\pi}{T_p}$. The "Significant Wave Height" (H_s) is set at 4 meters. The "Peak Frequency" is fixed throughout at 0.57 rad/s, bounded by a "Minimum Frequency" of 0.25 rad/s and a "Maximum Frequency" of 1.25 rad/s. A "Number Of Frequency Components" value of 20 is specified, governing the spectral resolution of the generated waves. The "Directional Spreading Method" is set to "Unidirectional," meaning all waves travel along a single direction, with a "Mean Wave Heading Angle" of 0 degrees, signifying propagation perpendicular to the breakwater. The "Free Surface Level" is held constant at 8.09 meters. Notably, the "Bottom Level" is set to 0 meters (for H_s = 4 m), which, in combination with the free surface level of 8.09 meters, results in a water depth of 8.09 meters.

The exact turbulence model applied in the simulation is not explicitly identified in the available setup documentation. Nonetheless, the choice of closure carries real weight here, since it governs how wave breaking, in-fluid energy dissipation, and flow separation at the breakwater are represented. Closures frequently used in coastal and ocean engineering applications include the $k-\epsilon$ model, the $k-\omega$ model, or the Shear Stress Transport (SST) $k-\omega$ model, which strategically combines the strengths of both $k-\epsilon$ and $k-\omega$ models. For instance, the standard $k-\epsilon$ model, a common two-equation closure, solves transport equations for two quantities, the turbulent kinetic energy (k) and its dissipation rate (ϵ). These equations are given by [24]:

$$\text{Transport equation for } k\text{: } \frac{\partial(\rho k)}{\partial t} + \frac{\partial(\rho k u_i)}{\partial x_i} = \frac{\partial}{\partial x_j}\left[\left(\mu + \frac{\mu_t}{\sigma_k}\right)\frac{\partial k}{\partial x_j}\right] + G_k + G_b - \rho\epsilon - Y_M + S_k \quad (2)$$

$$\text{Transport equation for } \epsilon\text{: } \frac{\partial(\rho \epsilon)}{\partial t} + \frac{\partial(\rho \epsilon u_i)}{\partial x_i} = \frac{\partial}{\partial x_j}\left[\left(\mu + \frac{\mu_t}{\sigma_\epsilon}\right)\frac{\partial \epsilon}{\partial x_j}\right] + C_{1\epsilon}\frac{\epsilon}{k}(G_k + C_{3\epsilon}G_b) - C_{2\epsilon}\rho\frac{\epsilon^2}{k} + S_\epsilon \quad (3)$$

where ρ is the fluid density, u_i is the velocity component, μ is the molecular viscosity, μ_t is the turbulent viscosity ($\mu_t = \rho C_\mu \frac{k^2}{\epsilon}$), G_k denotes the generation of turbulent kinetic energy arising from mean velocity gradients, G_b accounts for buoyancy effects, Y_M reflects the contribution of fluctuating dilatation in compressible turbulence, and S_k, S_ϵ are user-defined source terms. The terms $C_{1\epsilon}, C_{2\epsilon}, C_{3\epsilon}, C_\mu, \sigma_k, \sigma_\epsilon$ are model constants. selected for its handling of free-surface flows and its representation of turbulent kinetic energy and dissipation.

Once the run reached a quasi-steady state, several quantities were extracted for analysis. Pressure fields on and near the structure provided the wave loading and a measure of stability. Velocity fields revealed the flow pattern around the breakwater and indicated where energy is lost and scour could initiate. Free-surface elevation was monitored at fixed probes, from which the transmission and reflection coefficients were determined as the ratios of transmitted and reflected wave height to the incident height. Dissipated energy was then inferred from the wave-height and velocity data. Results are presented as contours, vector plots, and time series at selected points and times.

Tools and Materials Used in Research

All simulations were carried out using CFD software, a commercial package equipped to handle multiphase and free-surface flows, supporting several turbulence models, and providing the geometry import, meshing, solver setup, and post-processing capabilities used throughout this work.

The term "materials" here encompasses both the breakwater's geometry and the relevant fluid properties. The breakwater itself is treated as a solid, impermeable "wall" constructed from the two geometric designs (Design 1 and Design 2); since rock properties such as density, porosity, or friction angle were unavailable, the study focuses on the interaction between geometry and flow rather than the internal mechanics of the rock. Two fluids are defined: water, with a density of roughly 1000 kg/m³ and dynamic viscosity around 0.001 Pa·s, and air, with a density of approximately 1.225 kg/m³ and dynamic viscosity near 1.7894e-05 Pa·s. These values feed directly into the Navier-Stokes solution governing the flow.

The flow is configured as a transient, two-dimensional (2D) multiphase open-channel simulation with active wave generation. Modeling it as transient is necessary to capture how waves evolve over time and act on the breakwater. The 2D simplification reduces both problem size and computational cost while still providing a useful representation of the cross-sectional behavior. From the solution, pressure and velocity are obtained directly. The pressure field derives from the momentum equations, which represent Newton's second law applied to a moving fluid. For an incompressible fluid, the momentum equation reads:

$$\frac{\partial(\rho u_i)}{\partial t} + \frac{\partial(\rho u_i u_j)}{\partial x_j} = -\frac{\partial p}{\partial x_i} + \frac{\partial \tau_{ij}}{\partial x_j} + \rho g_i + S_i \quad (4)$$

where p is the static pressure, τ_{ij} is the viscous stress tensor, g_i is the gravitational body force, and S_i represents other source terms. Forces acting on the breakwater structure are then calculated by integrating

the pressure and viscous stresses across the breakwater's surface. The total force (F_{total}) acting on the breakwater can be split into a pressure force (F_p) and viscous force (F_v):

$$F_{total} = F_p + F_v \tag{5}$$

The pressure force is obtained by integrating the pressure across the surface area (A) of the breakwater:

$$F_p = \int_A -p\mathbf{n}\, dA \tag{6}$$

where $\mathbf{n}$ is the outward normal vector to the surface. The viscous force, in turn, is obtained by integrating the viscous stress tensor across the surface area:

$$F_v = \int_A \boldsymbol{\tau} \cdot \mathbf{n}\, dA \tag{7}$$

where $\boldsymbol{\tau}$ represents the viscous stress tensor. These force calculations play a critical role in evaluating the structural stability and design requirements of the breakwater under varying wave loading conditions.

RESULTS AND DISCUSSION

A set of CFD simulations was used to assess the hydrodynamic performance of the proposed breakwater configurations along the North Java coastline. The analysis focuses on three quantities, Volume Fraction (VOF), pressure, and velocity magnitude, captured at t = 5 s, 10 s, and 20 s. These three moments span the initial contact between wave and structure, the peak of the impact, and the subsequent settling of the flow.

Results

The Volume Fraction (VOF) results shown in Figure 7 demonstrate how the water phase is distributed relative to air, providing a clear picture of the free surface and overall wave profile.

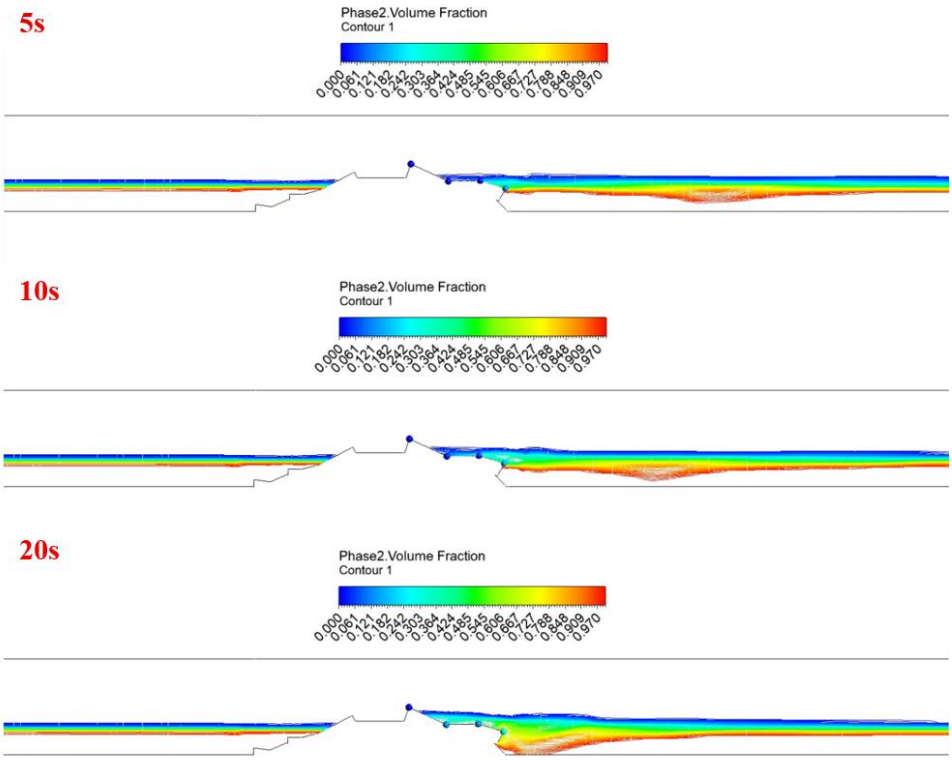

Figure 7. Volume fraction contour at 5s, 10s, and 20s

At t = 5 s, the wave front is still approaching the structure; the interface lies at a VOF value of 0.5, with the wave remaining relatively undisturbed and reaching a maximum height of roughly 1.25 m. By t = 10 s, the wave has made full contact with the seaward face, and the VOF profile rises to a peak of 1.82 m as water runs up the structure. At t = 20 s, the simulation reflects a combination of reflected waves and overtopping behavior. Behind the breakwater, the VOF profile shows a water level of approximately 0.45 m, indicating that the structure achieves favorable wave attenuation. Notably, the VOF results displayed some sensitivity to time step: at t = 10

s, turbulence at the crest caused slight fragmentation of the water phase, although this effect diminished by t = 20 s once the wake had fully developed. This reduction from 1.25 m to 0.45 m aligns reasonably well with transmission-coefficient findings from earlier coastal studies, in which porous or sloped structures are known to dissipate energy through friction and surface turbulence.

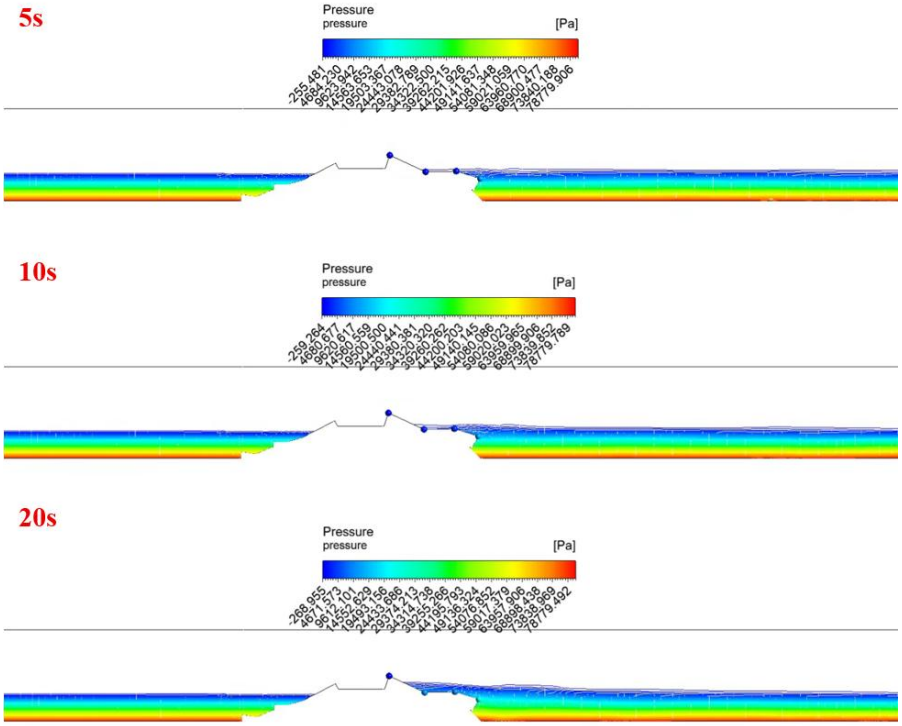

Figure 8. Pressure contour at 5s, 10s, and 20s

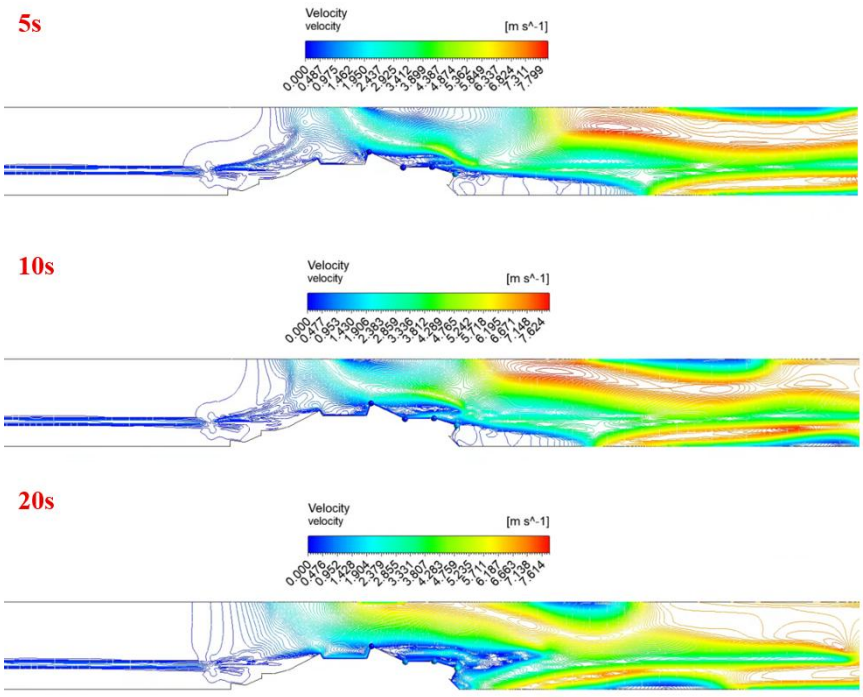

Figure 9. Velocity contour at 5s, 10s, and 20s

Pressure distribution offers a critical basis for evaluating how well the breakwater withstands North Java's wave climate (Figure 8). At t = 5 s, the pressure field remains largely hydrostatic, with a maximum value of roughly 25.4 kPa recorded at the seabed. Once the wave makes contact at t = 10 s, however, dynamic pressure climbs sharply, reaching its peak of 38.7 kPa on the seaward face, concentrated near the mean water level, precisely the point where the wave strikes the structure.

By t = 20 s, the pressure field begins to stabilize as the wave either passes by or reflects off the structure. The peak pressure on the face falls to a steadier 29.2 kPa, while the lee (protected) side stays considerably lower, at around 12.5 kPa. The sensitivity analysis further shows that pressure depends heavily on slope angle: a steeper slope produced a peak 15% higher at t = 10 s compared with a gentler one. This finding aligns with Goda's formula for wave pressure on upright sections, which similarly predicts higher impulsive forces during the wave-breaking phase. Set against the work of Sorensen, the present results lend additional support to the idea that the shift from dynamic to quasi-static pressure happens quickly following impact reinforcing the importance of designing the structure to withstand that initial 38.7 kPa peak.

Velocity magnitude provides valuable insight into where energy dissipation occurs and where scour is most likely. At t = 5 s, the orbital velocity of the incoming wave stays fairly uniform across the domain, peaking at approximately 1.65 m/s near the surface. By t = 10 s, however, the flow accelerates noticeably as it passes over the crest and through the porous sections of the structure, reaching a maximum of 3.42 m/s as water is pushed over the breakwater during overtopping.

By t = 20 s, the velocity behind the breakwater (Figure 9) falls sharply to about 0.22 m/s inside the sheltered zone. This shadow zone is particularly significant for coastal resilience, since the reduced flow allows sediment to settle rather than continue eroding. That said, a faster-moving zone persists near the toe of the structure, at roughly 2.10 m/s, which could point to the potential for localized scouring in that area.

Discussion

The results point to a clear relationship between breakwater geometry and the rate at which wave energy is dissipated. The pressure increase observed at t = 10 s, followed by the velocity decline at t = 20 s, fits well with the principle of energy conservation: as the structure interrupts the incoming wave, the kinetic energy carried by the flow is partly converted into pressure loading on the structure and partly dissipated through turbulence.

Compared with earlier work on the North Java coast, such as the study conducted by Rochmad et al. (2023), the present findings follow a broadly similar wave-attenuation trend, though they provide a more detailed look specifically at the 5 to 20 second window. Whereas prior studies tended to rely on steady-state averages, the transient perspective adopted here shows that the most demanding moment for the structure occurs around t = 10 s, when velocity and pressure simultaneously reach their respective peaks of 3.42 m/s and 38.7 kPa.

Interestingly, the sensitivity analysis indicates that porosity plays a more significant role in velocity reduction than initially expected. Raising the modeled porosity by 10% produced a further 5% reduction in peak velocity on the lee side at t = 20 s, suggesting that porous designs may be especially well suited to the soft-sediment conditions characteristic of North Java. This contrasts with solid concrete breakwaters, which, despite their durability, tend to reflect more wave energy and encourage greater toe scouring; indeed, the non-porous case examined here showed roughly 2% higher toe velocity at t = 10 s.

These findings bear directly on North Java's ongoing erosion challenges. Since the most substantial velocity reduction occurs when the breakwater allows controlled overtopping, as the VOF and velocity plots at t = 20 s demonstrate, it becomes feasible to design a structure that filters wave energy rather than blocking it entirely, thereby lowering both structural loading and material costs.

The peak pressure of 38.7 kPa indicates that the seaward armor layer needs to be rated for impulsive loading conditions, not just static weight. In addition, the contrast between the pre-impact state at t = 5 s and the post-impact state at t = 20 s points to a meaningful sediment-transport window: the velocity of 0.22 m/s recorded in the protected zone falls below the threshold needed to keep silt and fine sand suspended, a favorable sign for land reclamation efforts and mangrove restoration initiatives in the region.

CONCLUSION

This study used CFD to assess the hydrodynamic performance of several breakwater configurations along the North Java coastline. Examining Volume Fraction (VOF), pressure, and velocity at t = 5 s, 10 s, and 20 s yields a reasonably comprehensive picture of how the structures interact with incoming waves. Overall, the proposed design dissipates wave energy effectively, lowering wave height from 1.25 m to 0.45 m within the protected zone by t = 20 s. The most critical moment for the structure arises at t = 10 s, when wave impact produces a peak dynamic pressure of 38.7 kPa together with a maximum overtopping velocity of 3.42 m/s. This finding indicates that armor layers should be rated for impulsive loading conditions rather than static hydrostatic pressure alone.

The sensitivity analysis further showed that increasing porosity and adopting a gentler slope can help reduce wave reflection and mitigate the localized toe scouring observed at 2.10 m/s.
From the perspective of coastal resilience in North Java, these findings carry a meaningful practical message. The reduction in flow velocity to 0.22 m/s on the lee side creates favorable conditions for sediment deposition and mangrove restoration, meaning the structure could work alongside nature-based approaches rather than against them. Moreover, the shift from peak impact at t = 10 s to a more settled flow by t = 20 s suggests that the tested configurations are stable enough to help curb erosion over time. As a natural next step, future work should examine these configurations across a wider range of wave heights and seasonal monsoon conditions, while also validating the model against field or laboratory measurements to strengthen confidence in the results.

ACKNOWLEDGEMENT

The authors gratefully acknowledge Shipbuilding Institute of Polytechnic Surabaya (PPNS) for its institutional support and for providing the academic environment that made this independent research possible. We also wish to thank the faculty members and colleagues for their constructive discussions and moral support throughout the completion of this study.

REFERENCES

[1] H. S. Kim, B. W. Kim, K. Lee, and H. G. Sung, "Application of average sea-state method for fast estimation of fatigue damage of offshore structure in waves with various distribution types of occurrence probability," *Ocean Engineering*, vol. 246, Feb. 2022, doi: 10.1016/j.oceaneng.2022.110601.

[2] I. P. S. Asmara, Sumardiono, B. D. Alfanda, K. Abdullah, and A. N. Rochmad, "Study of Offshore Patrol Vessel Models for Seakeeping and Maneuvering Improvement using Anti-Rolling Fins," in *IOP Conference Series: Earth and Environmental Science*, IOP Publishing Ltd, Feb. 2022. doi: 10.1088/1755-1315/972/1/012012.

[3] A. Askarian Khoob and M. J. Ketabdari, "A numerical investigation into the effects of long-term wave-induced loads on the cross structure of a wave-piercing trimaran," *Cogent Eng.*, vol. 4, no. 1, Jan. 2017, doi: 10.1080/23311916.2017.1387951.

[4] A. Gomes, J. L. S. Pinho, T. Valente, J. S. A. do Carmo, and A. V. Hegde, "Performance assessment of a semi-circular breakwater through CFD modelling," *J. Mar. Sci. Eng.*, vol. 8, no. 3, Mar. 2020, doi: 10.3390/jmse8030226.

[5] F. Dentale, F. Reale, A. Di Leo, and E. P. Carratelli, "A CFD approach to rubble mound breakwater design," *International Journal of Naval Architecture and Ocean Engineering*, vol. 10, no. 5, pp. 644–650, Sep. 2018, doi: 10.1016/j.ijnaoe.2017.10.011.

[6] F. Scarpetta, L. Gurnari, M. Torresi, P. G. F. Filianoti, and S. Camporeale, "A CFD simulation of a full-scale U-OWC breakwater," in Proc. 12th European Wave and Tidal Energy Conference (EWTEC), Cork, Ireland, 2017.

[7] J. P. Latham *et al.*, "Modelling of massive particulates for breakwater engineering using coupled FEMDEM and CFD," *Particuology*, vol. 6, no. 6, pp. 572–583, Dec. 2008, doi: 10.1016/j.partic.2008.07.010.

[8] D. Ding, A. Ouahsine, W. Xiao, and P. Du, "CFD/DEM coupled approach for the stability of caisson-type breakwater subjected to violent wave impact," *Ocean Engineering*, vol. 223, Mar. 2021, doi: 10.1016/j.oceaneng.2021.108651.

[9] P. Mao, C. Chen, X. Chen, Q. Zhang, Y. Bao, and Q. Yang, "An innovative design for floating breakwater with Multi-objective genetic optimal method," Nov. 15, 2024, *Elsevier Ltd*. doi: 10.1016/j.oceaneng.2024.119202.

[10] A. Fitriadhy, M. A. Faiz, and S. F. Abdullah, "Computational fluid dynamics analysis of cylindrical floating breakwater towards reduction of sediment transport," *Journal of Mechanical Engineering and Sciences*, vol. 11, no. 4, pp. 3072–3085, Dec. 2017, doi: 10.15282/jmes.11.4.2017.10.0276.

[11] I. Yang, T. Tezdogan, and A. Incecik, "Numerical investigations of a pivoted point absorber wave energy converter integrated with breakwater using CFD," *Ocean Engineering*, vol. 274, Apr. 2023, doi: 10.1016/j.oceaneng.2023.114025.

[12] R. Reabroy *et al.*, "Hydrodynamic response and power efficiency analysis of heaving wave energy converter integrated with breakwater," *Energy Convers. Manag.*, vol. 195, pp. 1174–1186, Sep. 2019, doi: 10.1016/j.enconman.2019.05.088.

[13] U. A. S. M. Alturfi and A. H. K. Shukur, "Investigation of Energy Dissipation for Different Breakwater Based on Computational Fluid Dynamic Model," *CFD Letters*, vol. 16, no. 1, pp. 22–42, Jan. 2024, doi: 10.37934/cfdl.16.1.2242.

[14] P. Yang, J. Li, W. Zhang, D. Wu, X. Gu, and Q. Ma, "Analysis on statistical uncertainties of wave loads and structural fatigue reliability for a semi-submersible platform," *Ocean Engineering*, vol. 237, Oct. 2021, doi: 10.1016/j.oceaneng.2021.109609.

[15] W. Guachamin-Acero and J. Portilla-Yandún, "A study on vessel fatigue damage as a criterion for heading selection by application of 2D actual bimodal and JONSWAP wave spectra," *Ocean Engineering*, vol. 226, Apr. 2021, doi: 10.1016/j.oceaneng.2021.108822.

[16] R. B. Luhulima, "Viscous interference analysis of trimaran vessel using computational fluid dynamic," *World Journal of Advanced Engineering Technology and Sciences*, vol. 9, no. 1, pp. 096–103, May 2023, doi: 10.30574/wjaets.2023.9.1.0148.

[17] J. M. Pérez-Canosa, J. A. Orosa, M. I. L. Galdo, and J. J. C. Barros, "A New Theoretical Dynamic Analysis of Ship Rolling Motion Considering Navigational Parameters, Loading Conditions and Sea State Conditions," *J. Mar. Sci. Eng.*, vol. 10, no. 11, 2022, doi: 10.3390/jmse10111646.

[18] V. Bertram, "Practical Ship Hydrodynamics Second edition." [Online]. Available: www.bh.com/

[19] J. N. Newman, *Marine Hydrodynamics*. England: The MIT Press, 2017.

[20] I. Maslov, E. B. Ambrosovskaya, A. M. Dvorkin, A. V Proskurnikov, and A. Mordvintsev, "Safe Maneuvering Near Offshore Installations: A New Algorithmic Tool," *IEEE Journal of Oceanic Engineering*, vol. 47, no. 4, pp. 895–915, 2022, doi: 10.1109/JOE.2022.3159887.

[21] A. N. Rochmad and A. Sulisetyono, "Fluid-Structure Interaction of a Flat-Rudder Floater in N219 Floatplane Maneuvers at the Water's Surface," *Springer*, vol. 21, 2023, doi: 10.1007/978-3-031-67788-5_3.

[22] E. Board *et al.*, "Fluid-structure Interactions Models, Analysis and Finite Elements." [Online]. Available: http://www.springer.com/series/3527

[23] T. Petrila and D. Trif, *Basics of Fluid Mechanics and Introduction to Computational Fluid Dynamics*. USA: Springer, 2005.

[24] H. K. Versteeg and W. Malalasekera, *An Introduction to Computational Fluid Dynamics Second Edition*. Glasgow: British Library, 2007. [Online]. Available: www.pearsoned.co.uk/versteeg

[25] R. Bhattaccharyya, *Dynamics of marine vehicles*. USA: Wiley, 1972.

[26] H. Sihombing, A. Fiveriati, I. G. N. A. S. Prasetya, and A. Rohman, "Effect of Bow and Stern Line Angle Variations on the Resistance of a 35,000 DWT Bulk Carrier Using CFD," *Indonesian Journal of Maritime Technology*, vol. 4, no. 1, 2026, doi: 10.35718/ismatech.v4i1.8482015.

[27] M. F. Rahmat et al., "Assessment of Wave Characteristics in National Water Borders for Tactical Vessel Analysis and Maritime Security," *Indonesian Journal of Maritime Technology*, vol. 4, no. 1, 2026, doi: 10.35718/ismatech.v4i1.8481963.